THE ASTROPHYSICAL JOURNAL, 281: 225–236, 1984 June 1

FAR-INFRARED SELECTED STAR FORMATION REGIONS

D. T. JAFFE,[1,2] R. H. HILDEBRAND,[2,3] AND JOCELYN KEENE[2,4]
Enrico Fermi Institute, University of Chicago

D. A. HARPER AND R. F. LOEWENSTEIN
Yerkes Observatory, University of Chicago

AND

J. M. MORAN[5]
Harvard-Smithsonian Center for Astrophysics
Received 1983 August 29; accepted 1983 November 29

ABSTRACT

We present detailed far-IR observations and complementary submillimeter, 5 GHz continuum and $C^{18}O$ observations of a sample of eight far-IR selected luminous regions of star formation. The observations show that the sources of luminosity coincide with density peaks in the molecular clouds and that the exciting stars lie deep within these condensations. The far-IR sources have diversely shaped 40–180 μm spectra even though their 60–100 μm color temperatures are similar. The radio and far-IR results together show that the exciting stars are in clusters containing either zero-age main-sequence and pre–main-sequence stars or consisting entirely of pre–main-sequence objects. $C^{18}O$ and submillimeter observations imply gas densities $\sim 10^5$–high enough to make $T_{dust} \sim T_{gas}$.

Subject headings: interstellar: molecules — stars: formation — stars: pre–main-sequence

I. INTRODUCTION

The current sample of well-studied luminous galactic far-IR sources, especially those selected from radio continuum (e.g., Thronson and Harper 1979) or ^{12}CO $J = 1$–0 line mapping (e.g., Evans *et al.* 1982), may not provide an unbiased picture of the nature of luminous far-IR sources in general. Radio continuum surveys require the presence of nearby hot stars, generally of type O9 or earlier. Surveys in optically thick molecular lines like ^{12}CO require that the embedded sources either be very luminous or lie close to the front edges of molecular clouds. In addition, published studies either survey many sources using one technique or study individual sources in more detail. The aim of this investigation is to address both of these problems by making detailed infrared, submillimeter, radio continuum, and CO observations of a far-IR selected source sample.

We chose eight sources from the far-IR survey of Jaffe, Stier, and Fazio (1982, hereafter JSF) for detailed study. Five of these, (12.4+0.5, 12.8+0.3, 12.9+0.5, 12.9+0.3 [W33A], and 14.3−0.6) were the brightest (S_ν[70 μm] $\geq$ 1700 Jy), and most compact ($\vartheta \leq 1'$), 70 μm sources from that survey with little or no ($\leq$100 mJy) associated radio continuum emission. We also investigated 12.7−0.2 (W33B) which we (correctly) suspected would be compact when observed with a small beam, even though the total 5 GHz radio continuum within 30″ of this source is 0.6 Jy (Wynn-Williams, Beichman, and Downes 1981). The two remaining sources (12.4−1.1 and 14.4−0.7) have similar far-IR characteristics to the first five but lie near extended (2′–3′ diameter) H II regions.

We wished to determine whether far-IR selected objects with low radio continuum fluxes differed from objects selected in other ways and whether these sources had far-IR spectral or structural characteristics that would be useful as predictors of their other properties. In addition, we wished to understand the nature of the stars or protostars that provide the luminosity. We also hope to resolve two questions about compact far-IR objects near radio continuum sources: Where is the far-IR emission that should be associated with the H II region? Do the compact far-IR sources near H II regions differ from the other compact sources?

We discuss the observing techniques in § II, the characteristics of the individual sources in § III, and the properties of the sources as determined by the different types of observations in § IV. In § V, we give a synthesis and summary of the results.

II. OBSERVATIONS

a) Far-IR Observations

We observed the eight sources from the JSF survey listed in Table 1 in the far-infrared with the 0.91 m telescope of the Kuiper Airborne Observatory in 1981 May and 1982 May. In 1981, we used the pumped ^{4}He cooled Yerkes Observatory G-2 photometer and in 1982 we used the G-2 system and the Yerkes ^{3}He cooled H-1 system (Harper *et al.* 1984). Table 2 lists the half-power wavelength and the effective wavelength for each of the filter/aperture combinations. We calculated the effective wavelengths assuming a source spectrum like that of FIR 12.4+0.5 (Fig. 1). The G-2 system has an array of seven Winston light collectors (Harper *et al.* 1976) followed by bolometers in integrating cavities. The collectors lie in a close-packed hexagonal pattern with 55″ between beam centers on the sky. The system has two aperture sizes: 49″ and 33″. The H-1 system permits sensitive observations through well-

[1] Now at Space Sciences Laboratory, University of California, Berkeley.
[2] Visiting Astronomer at the Infrared Telescope Facility which is operated by the University of Hawaii under contract from the National Aeronautics and Space Administration.
[3] Also at Department of Astronomy and Astrophysics and Department of Physics, The University of Chicago.
[4] Now at Division of Physics, Mathematics and Astronomy, California Institute of Technology.
[5] Visiting Astronomer, Radio Astronomy Laboratory, University of California, 1982–1983.

TABLE 1

FAR-INFRARED POSITIONS AND SIZES

Source (1)	60 μm Position R.A. (1950) (±10″) (2)	60 μm Position Decl. (1950) (±10″) (3)	H_2O Maser Position[a] R.A. (1950) (4)	H_2O Maser Position[a] Decl. (1950) (5)	Error (arcsec) (6)	60 μm Size[b] (33″ beam) (arcsec) (7)	100 μm Size (31″ beam) (arcsec) (8)	180 μm Size (51″ beam) (arcsec) (9)
12.4+0.5	18h07m55s6	−17°56′33″	18h07m56s4	−17°56′37″	10	<15	24	28
12.9+0.5	18 08 56.6	−17 32 22	18 08 56.3	−17 32 16	10	15	18	<25
12.8+0.3	18 09 17.4	−17 42 49	18 09 15.6	−17 43 35	4	36	42	36
12.7−0.2 (W33B)	18 10 59.5	−18 02 31	18 10 59.24	−18 02 40.9[c]	0.3	17	41	37
12.9−0.3 (W33A)	18 11 44.2	−17 52 56	18 11 44.0	−17 53 09	5	15	19	45
12.4−1.1	18 13 54.7	−18 42 33	18 13 56.1	−18 42 57	10	25	26	32
14.3−0.6	18 16 00.3	−16 49 08	18 16 00.8	−16 49 06	5	16	<15	24
14.4−0.7	18 16 22.6	−16 45 20[d]	...	...	...	68[e]	73[e,f]	71[e,g]

[a] Jaffe, Guesten, and Downes 1981.
[b] All sizes are deconvolved assuming Gaussian beam shapes (33″ at 60 μm and 31″ at 100 μm, 51″ at 180 μm) and Gaussian source intensity distributions.
[c] Lada *et al.* 1981.
[d] Position derived from a single observation with the G-2 array and a 49″ beam at 62 μm.
[e] Size derived from a single observation with the G-2 array and a 49″ beam.
[f] Mean wavelength is 116 μm for this point.
[g] Mean wavelength is 160 μm for this point.

defined bandpasses at wavelengths from 100 μm to 200 μm (see Table 2). With this system, we used apertures with sizes of 31″, 51″, and 87″. In 1981 the separation of signal and reference beams was 7′.5–9′, and the frequency was 30 Hz. In 1982 the separation was 4′.5–5′.5, and the frequency was 27 Hz. We pointed the telescope by keeping a guide star (≤5′ away) centered in a computer-controlled focal plane offset guider. We knew the positions of the offset stars to ±1″ and estimated guiding errors of ~±5″ and offsetting errors of about the same order. Overall, we determined the far-IR positions to ±10″.

We calibrated the far-IR intensities using the iterative reduction scheme described in the Appendix. An onboard zenith water vapor radiometer (Kuhn, Magaziner, and Stearns 1976) provided estimates of the line-of-sight H_2O during the observations. We estimate that the overall error in the flux density scale is ±25%. The relative source-to-source and color errors are considerably smaller.

For all sources except FIR 14.4−0.7, we determined the positions and sizes by making cross scans at 60 μm and 100 μm with 33″ and 31″ beams and at 180 μm with a 51″ beam. The cross scans were in elevation and cross-elevation (within ~15° of north-south, east-west, respectively) and covered 63″ on either side of the source center in 15″.7 steps (1 mm at the focal plane). We derived the source sizes by assuming Gaussian shapes for the sources and the beams. The uncertainties in the source sizes are ~±10% of the beam sizes (1 σ) for sources the same size as the beam. We mapped FIR 12.8+0.3 at 100 μm with a 31″ beam (Fig. 2) by making repeated line scans sampling every 15″.7 along lines spaced by 15″ in elevation. We mapped FIR 14.4−0.7 at 120 μm with the G-2 system using 49″ apertures and a low pass filter with a cut-on wavelength of 85 μm (Fig. 3) and 12.4−1.1 at 100 μm with the G-2 photometer using the filter described in Table 2. We also made a partial

TABLE 2

FAR-INFRARED FILTERS AND APERTURES

Filter	Beam Size (arcsec)	Effective Wavelength (12.4 + 0.5 Spectrum) (μm)	$\lambda_{cut\text{-}on}$ (μm)	$\lambda_{cut\text{-}off}$[a] (μm)
Yerkes G2 – 7 Channel Array				
1	33	38	31	52
1	49	38	31	52
2	33	59	48	75
2	49	59	48	75
4	49	111	78	∞
6	49	102	82	121
Yerkes H1 Single Channel He^3 System				
1	31	104	91	125
3	51	136	125	155
5	51	162	183	235
7	51	174	156	295
7	87	181	156	295

[a] The cut-on and cut-off wavelengths are the 50% transmission points of the filters, not allowing for diffraction, atmospheric transmission or the form of the source spectrum.

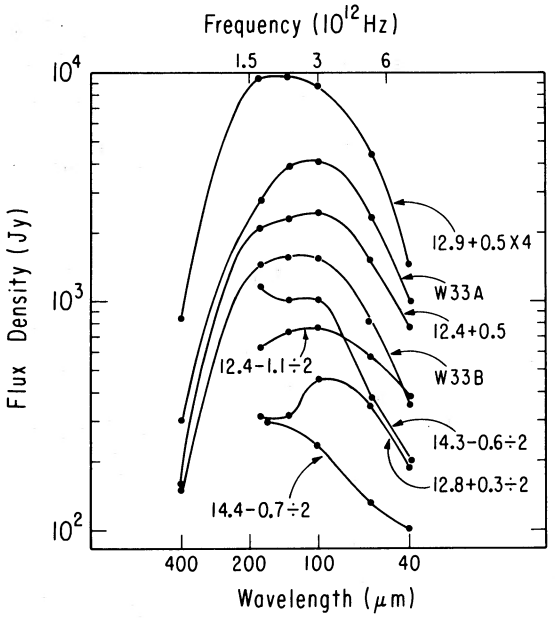

FIG. 1.—Far-IR spectra of the eight sources in our sample. These spectra were taken with 49″–50″ beams toward the 60 μm peaks of the sources. The absolute errors in the fluxes are dominated by the calibration (±25%). The solid lines serve only to connect the data points.

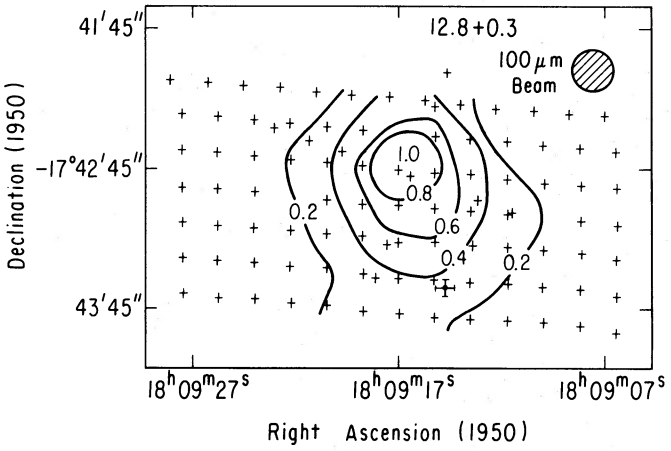

FIG. 2.—100 μm map of far-IR 12.8+0.3. The beamsize was 31″. The light crosses represent individual data points. The heavy barred cross gives the position and positional uncertainty of the H_2O maser (Jaffe, Guesten, and Downes 1981). The contour levels are relative to the peak flux density (600 Jy per beam, peak surface brightness = 2.3×10^{-16} W m^{-2} Hz^{-1} sr^{-1}.

map of FIR 14.4−0.7 with the H-1 system at 185 μm with an 87″ beam.

Table 1 gives the 60 μm positions and the 60 μm, 100 μm, and 180 μm sizes of the far-IR sources as well as the positions of associated H_2O maser emission centers (Jaffe, Guesten, and Downes 1981). Table 3 lists the linear size, far-IR luminosity, dust temperatures, and optical depths. Figure 1 shows far-IR spectra of the eight sources, and Figure 4 shows representative cross scans of some of the sources.

b) Submillimeter Observations

We made submillimeter continuum (sub-mm) observations of some of the far-IR sources in 1981 June and November and 1983 March with the University of Chicago sub-mm photometer (Whitcomb, Hildebrand, and Keene 1980) on the 3 m NASA Infrared Telescope (IRTF) on Mauna Kea, Hawaii. The beam diameter was 48″ (full width at half-maximum) in 1981 and 35″ in 1983. The chopping secondary mirror gave a beam separation of 300″. A low-frequency pass filter (Whitcomb and Keene 1980) and diffraction by the field optics and telescope fixed the limits of the instrumental spectral passband at 300 μm and 800 μm. The flux-weighted mean wavelength, taking into account atmospheric transmission and the source spectra, was ~400 μm. We determined the fluxes of the sources relative to W33A, the flux of which we had determined relative to Jupiter and Saturn (Hildebrand *et al.* 1984). We made additional sub-mm observations in 1983 April with the 3.6 m Canada-France-Hawaii telescope and the same photometer. For these observations, the beam size was 40″ and the chopper throw was 130″. Table 4 gives the observed and derived parameters from the submillimeter observations.

c) VLA Observations

We observed five of the sources in the present study and three additional far-IR sources from the JSF survey (see Table 5) in the 6 cm radio continuum with the VLA[6] in 1981 January.

[6] The VLA and 36 foot (11 m) telescopes are facilities of the National Radio Astronomy which is operated by Associated Universities, Inc. under contract with the National Science Foundation.

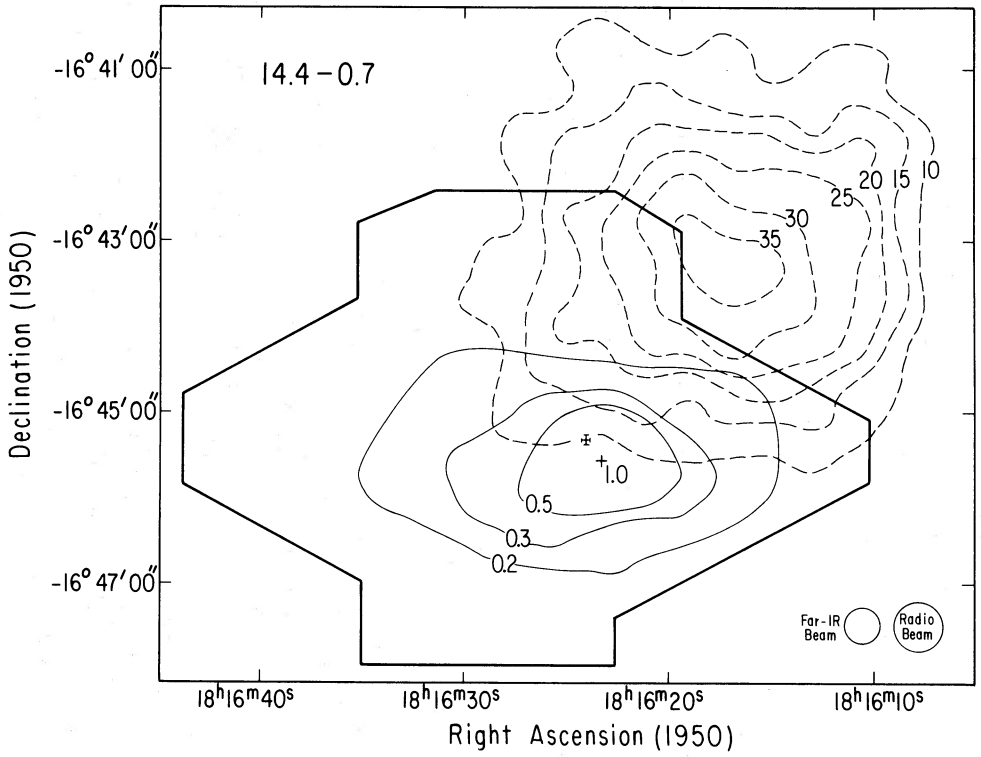

FIG. 3.—120 μm 49″ resolution map of far-IR 14.4−0.7 (*light lines*) superposed on a 10.7 GHz continuum map (Stier *et al.* 1982; *dashed lines*). The heavy lines show the outline of the region mapped at 120 μm. The cross gives the position of the far-IR peak. The barred cross gives the position and position error of the 10 μm source. The peak flux density at 120 μm is 570 Jy per beam (peak surface brightness = 8.9×10^{-17} W m^{-2} Hz^{-1} sr^{-1}). One contour unit in the radio map corresponds to 4.5 mJy per 70″ beam or 3.5×10^{-22} W m^{-2} Hz^{-1} sr^{-1}.

TABLE 3

FAR-INFRARED DERIVED PARAMETERS

Source (1)	Distance (kpc) (2)	100 μm Size (10^{17} cm) (3)	Luminosity in 49″ Beam (10^4 $L_\odot$) (4)	Total Far-IR Luminosity (30–1000 μm) (10^4 $L_\odot$) (5)	$T_{60\ \mu m-100\ \mu m}$ (νB_ν, 49″ Beam) (K) (6)	$\tau_{100\ \mu m}$ (31″ beam) (7)
12.4+0.5	2.3	8	2.0	2.3	39	0.08
12.9+0.5	3.6	10	3.9	4.4	36	0.21
12.8+0.3	2.3	14	0.8	1.3	42	0.02
12.7−0.2 (W33B)	4.9	30	5.2	6.7	36	0.05
12.9−0.3 (W33A)	3.7	11	8.0	8.9	38	0.15
12.4−1.1	4.1	16	4.6	5.9	42	0.03
14.3−0.6	2.3	<5	1.4	1.5	32	0.08
14.4−0.7	2.3	25	0.4	1.4	37	0.01[a]

[a] Measured with a 49″ beam.

The array was in its largest ("A") configuration, with 24 functioning antennas and a maximum baseline of 35 km. At the observing wavelength, the naturally weighted synthesized beam was ~0.″55 by 0.″85 (R.A. × decl.). We observed each source for a total of 45 minutes in 5 minute segments over a period of 9 hours. Fluxes were calibrated relative to 3C 286 and bootstrapped to a phase and position source near the program sources. The secondary calibrator was observed for 5 minutes out of every 25. We have conservatively estimated the maximum flux density of an undetected point source at field center U_0 to equal twice the peak noise in the inner 120″ diameter field. The corresponding limit for a source of arbitrary diameter ϑ (if the map is smoothed to a resolution equal to ϑ) and distance from the field center D (in arc seconds), is then

$$U \sim U_0(\vartheta/\vartheta_{\rm beam})e^{\ln 2(D/50)^2} . \quad (1)$$

The fields containing the far-IR sources were far (>10′) from strong (>150 mJy), compact (<2′) radio continuum sources. This isolation makes the upper limits derived from Table 5 and equation (1) reliable values for those fields.

Table 5 gives a summary of 70″ resolution 2.8 cm radio continuum observations of the eight far-IR sources (JSF), and the position of the VLA field center and the value of U_0 for each field. Table 6 lists the observed and derived parameters of the 6 cm continuum sources detected with the VLA. Figure 5 is a map of the 6 cm emission from the center of the 12.4+0.5 field.

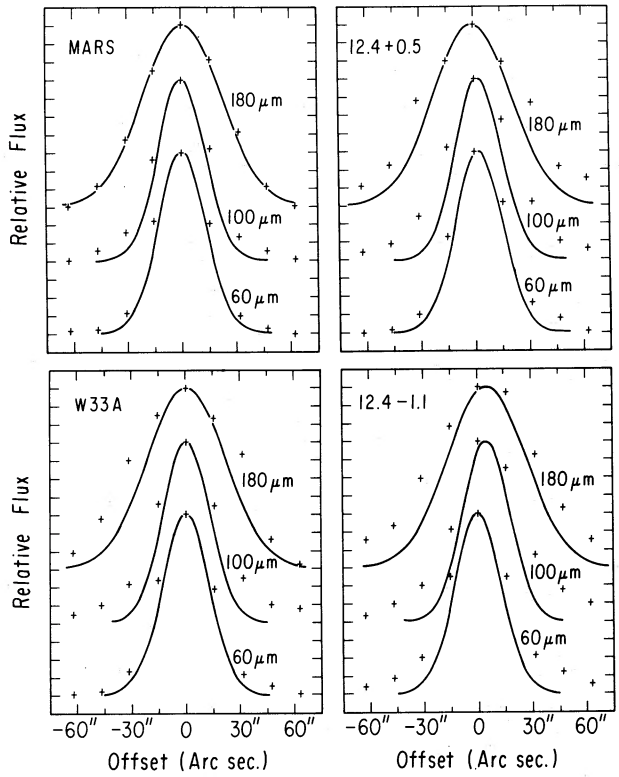

FIG. 4.—Cross scans of Mars and three far-IR sources at 60 μm, 100 μm, with 180 μm (*crosses*) superposed on idealized beam patterns (Gaussians with full widths to half-maximum equal to the deconvolved values listed in Table 2). Mars had a diameter of 12″ at the time of the observations.

d) CO *Observations*

We observed the $J = 1$–0 transitions of CO, ^{13}CO, and C^{18}O toward six of the far-IR sources in 1981 April and 1982 March with the NRAO 36 ft. telescope. We observed each line separately with a dual-channel cooled receiver followed by two 128 channel banks of 100 kHz filters (resolution ~0.27 km s^{-1}). The spectra consist of position-switched observations of the sources and reference positions away from the galactic plane which we had determined to have no significant amount of CO emission in the velocity range of interest. We used the chopper wheel method of Ulich and Haas (1976) to calibrate the data with M17SW as a reference source. Table 7 gives the observed parameters of the ^{12}C^{18}O $J = 1$–0 line toward the six sources and derived column densities and masses. Figures 6*a* and 6*b* show CO spectra toward FIR 12.9+0.5 and a position near W33A, respectively.

III. REMARKS ON INDIVIDUAL SOURCES

12.4+0.5.—Wright *et al.* (1979) first detected 70 μm emission from a ~30″ diameter source at this position. Beichman (1979) found a 10–20 μm source within the error box of the 70 μm source and Jaffe, Guesten, and Downes (1981) detected H_2O maser emission from the same region. The present observations show that the source diameter is 24″ (~8 × 10^{17} cm) at 100 μm and that the far-IR dust temperature is 38 K, assuming a λ^{-1} dust emissivity law. Coincident with the far-IR and near-IR sources are two 6 cm continuum sources (one optically thin and one unresolved) which lie ~5″ apart (Fig. 5). These sources account for at least half of the 2.8 cm continuum emission observed in a 70″ beam by JSF. The C^{18}O integrated line

TABLE 4

SUBMILLIMETER RESULTS

Source (1)	Total 400 μm Flux Density (Jy) (2)	400 μm Size (arcsec) (3)	Peak τ_{400} (4)	Peak A_v (5)	Peak n_{H_2} (10^5 cm^{-3}) (6)	M ($M_\odot$) (7)
12.4+0.5	220	24	0.04	230	3	400
12.9+0.5	240	18[a]	0.08	500	5	1300
12.8+0.3	190	36[b]	0.01	75	0.6	300
12.7−0.2 (W33B)	240	37[b]	0.02	120	0.4	2400
12.9−0.3 (W33A)	460	42	0.03	160	0.7	2400
12.4−1.1	120	32[b]	0.01	60	0.2	600

[a] We assume source size = 100 μm size.
[b] We assume source size = 180 μm size.

TABLE 5

VLA OBSERVATIONS

Source (1)	2.8 cm SINGLE DISH POSITION R.A. (1950) (2)	2.8 cm SINGLE DISH POSITION Decl. (1950) (3)	2.8 cm Size (arcmin) (4)	2.8 cm Flux Density (mJy) (5)	VLA Field Center R.A. (1950) (6)	VLA Field Center Decl. (1950) (7)	U_0, 6 cm Point Source Upper Limit[a] (mJy) (8)
12.4+0.5	$18^h07^m54^s.5$	−17°56′50″ ± 30″	<1.0	18 ± 6	$18^h07^m55^s.8$	−17°56′32″	[b]
12.9+0.5	...	...	...	<27	18 08 57.0	−17 32 20	0.8
12.8+0.3	18 09 16.3	−17 43 44 ± 30	2.5	136	18 09 16.0	−17 43 30	1.0
14.3−0.6	...	...	...	<40	18 16 00.0	−16 49 00	[b]
14.4−0.7	18 16 16.9	−16 43 20 ± 20	3.2	1200	18 16 24.0	−16 45 15	0.8
Other sources:							
13.7−0.6	...	...	...	<35	18 14 30.0	−17 23 20	1.4
14.1−0.6	18 15 15.5	−16 58 20 ± 40	<1.0	18 ± 9	18 15 14.0	−16 58 28	1.0
14.6−0.6	...	...	...	<27	18 16 22.0	−16 31 24	0.9

[a] The upper limits for point sources at field center are twice the peak to noise. The upper limit for a source of size θ, D arcsec from the field center U is given in eq. (1).
[b] See VLA results in Table 6.

TABLE 6

VLA RESULTS: 6 CENTIMETER CONTINUUM DETECTIONS

Source (1)	R.A. (1950) (2)	Decl. (1950) (3)	Diameter (arcsec) (4)	Flux Density (mJy) (5)	Number of Lyman Continuum Photons (10^{45} s^{-1}) (6)	n_e (10^3 cm^{-3}) (7)
12.4+0.5A	$18^h07^m55^s.37$	−17°56′34″.0 ± 0″.5	<0.8	1.2 ± 0.2	0.6	>12
12.4+0.5B	18 07 55.69	−17 56 31.0 ± 0.5	1.1	6.6 ± 0.7	3.3	18
14.3−0.6A	18 15 59.5	−16 48 59 ± 1	3	4.0 ± 1.0	2.0	3
14.3−0.6B	18 16 00.4	−16 49 06 ± 1	2	1.0 ± 0.3	0.5	3

TABLE 7

$^{12}C^{18}O$ RESULTS

Source (1)	T_A^* (K) (2)	V_{LSR} (km s^{-1}) (3)	ΔV (km s^{-1}) (4)	$\int T_A^* dV$ (K km s^{-1}) (5)	$\tau_{C^{18}O}$ $T_{ex} = T_{DUST}$ (6)	$N_{C^{18}O}$ (10^{16} cm^{-2}) (7)	n_{H_2}[a] (10^5 cm^{-3}) (8)	M Central Beam ($M_\odot$) (9)
12.4+0.5	2.1	18.5	2.2	6.4	0.09	2.3	1.6	1200
12.9+0.5	3.1	33.2	3.5	11.7	0.15	4.0	>1.8	5000
12.8+0.3	1.7	18.6	1.9	4.0	0.06	1.4	0.7	710
12.7−0.2 (W33B)	3.1	54.7	6.4	16.9	0.10	3.9	0.9	9000
12.9−0.3 (W33A)	4.2	35.8	5.3	20.8	0.18	7.1	1.7	9300
14.3−0.6	3.0	22.1	3.2	10.3	0.15	2.9	2.1	1500

[a] We assume that the source size is equal to the 180 μm continuum size. We also assume $N_{H_2} = 6 \times 10^6 N_{C^{18}O}$, the mean of the Taurus and Ophiucus values obtained by Frerking, Langer, and Wilson 1982. This is within 5% of the abundance one obtains by assuming solar abundance for carbon and a terrestrial $^{16}O/^{18}O$ value and that 10% of all carbon is in CO.

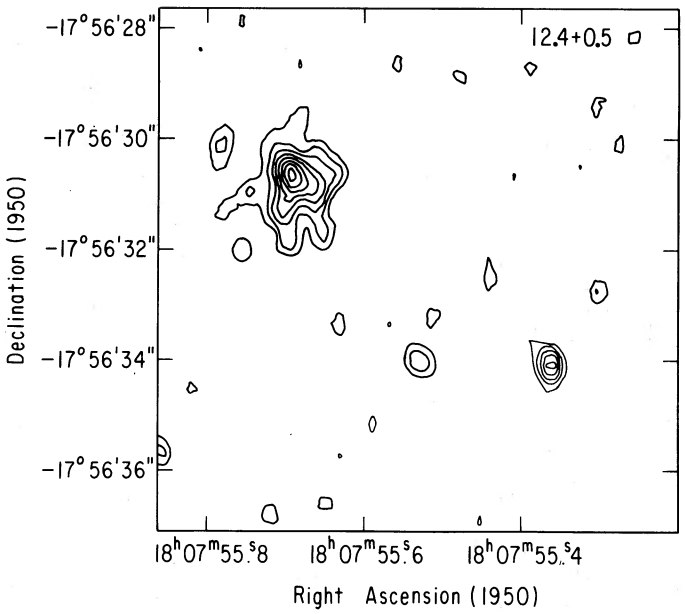

FIG. 5.—5 GHz VLA radio continuum map of G12.4+0.5. The contours are 0.2, 0.3, 0.4, 0.5, 0.6, 0.7, 0.8, and 0.9 of the peak flux density (1.5 mJy per beam).

strength distribution peaks sharply in the direction of the source and has a deconvolved full width to half-maximum (FWHM) equal to 110″.

12.8+0.3.—This is the only far-IR source with a far-IR peak position significantly different (53″ ± 11″) from the position of an associated H_2O maser (see Fig. 2). While the total far-IR luminosity is $1.3 \times 10^4\ L_\odot$, the luminosity in a 30″ beam centered on the maser position is only $1\text{–}1.5 \times 10^3\ L_\odot$.

12.7−0.2 (W33B).—This source has a Gaussian FWHM of ∼40″ at 100 μm. The large size derived by JSF (1.′5 × 3.′5) with a beam with 4 times the solid angle of our 100 μm beam probably refers to the extended emission associated either with this source or with the foreground W33 complex. The $C^{18}O$ results establish that the bulk of the molecular material toward W33B lies at 55 km s^{-1} and not at the 36 km s^{-1} velocity which dominates the rest of the W33 complex. The 55 km s^{-1} $C^{18}O$ integrated line strength clearly peaks at the far-IR source position. These results confirm the earlier NH_3 work of Ho, Martin, and Barrett (1981) demonstrating that W33B lies behind the W33 complex. Downes *et al.* (1984) have detected faint (5 Jy) 20 μm continuum emission toward the H_2O maser which lies close to the center of the far-IR emission.

12.9−0.3 (W33A).—This far-IR source has no detectable radio continuum flux (<5 mJy; Wynn-Williams, Beichman, and Downes 1981) even though its luminosity is $9 \times 10^4\ L_\odot$. A single main-sequence star with this luminosity surrounded by an optically thin H II region would produce a radio continuum flux density of 1.7 Jy at the distance of W33A. The far-IR emission region contains a near-infrared source with a high 3.5–12 μm blackbody color temperature (470 K), a low 20–33 μm temperature (53 K), and a deep 9.7 μm silicate feature. The near-IR results imply that a large amount of cooler dust overlies the hot central source. The far-IR and sub-mm results support such a conclusion, since the 60 μm source size is ∼15″, whereas the source size at 180 μm and 400 μm is ∼45″. The CO observations also suggest a hot core surrounded by dense cooler material. The ^{12}CO line gives no indication of the presence of the far-IR source (Jaffe 1980; Goldsmith and Mao 1983). At one point in the five point $C^{18}O$ map of W33A (7″W, 54″N of the far-IR position), there is a clear depression at the center of the ^{13}CO $J = 1\text{–}0$ emission profile (Fig. 6*b*). The $C^{18}O$ profile peaks at the velocity of this depression.

14.4−0.7.—Jaffe (1980) detected only four 10 μm sources at flux densities ≥9 Jy in his search for near-IR counterparts to the 42 JSF far-IR sources. Of these, only the source associated with 14.4−0.7 was previously unknown. The far-IR source is also the lowest luminosity source in the JSF survey with a near-IR counterpart at $S_\nu(10\ \mu m) > 9$ Jy. The far-IR source lies at the edge of an extended (3.′2 FWHM; Stier *et al.* 1982) H II region (Fig. 3). The VLA upper limit of 0.8 mJy for compact 6 cm continuum sources at the position of the far-IR and near-IR peaks implies a Lyman continuum photon flux $\leq 6 \times 10^{44}$ s^{-1} from embedded stars surrounded by optically thin compact H II regions. This upper limit and the observed far-IR luminosity are consistent with excitation by a cluster of three zero-age main-sequence (ZAMS) B2 stars (Panagia 1973). If a single star in its center excites the extended H II region, this star can account for $3 \times 10^3\ L_\odot$ (∼25%) of the luminosity inside the 30% contour of the far-IR source. If a cluster of ZAMS stars excites the H II region, heating by these stars could account for an even larger fraction of the luminosity of the far-IR source. The near-IR source would then account for the remaining 6000–8000 $L_\odot$. The measurements toward the far-IR peak with the G-2 photometer show that the dust temperature decreases both away from the near-IR source and away from the center of the H II region, indicating that heating from both plays a role in the far-IR emission.

IV. DISCUSSION

a) Far-IR Properties

i) *General Remarks*

All of the sources we observed as part of the present study were resolved either at 60 μm and/or 100 μm with a 30″ beam or at 180 μm with a 50″ beam. Figure 4 shows representative scans through some of the sources and through Mars at all three wavelengths superposed on the idealized (Gaussian) beam profile. Most sources show no significant trend toward larger sizes at longer wavelengths. The most notable exceptions are W33A and W33B which may be embedded in or (in the case of W33B) lie behind cooler extended emission from the W33 complex (Stier 1979), which would make the apparent source sizes larger at longer wavelengths. At the available resolution, all of the sources have single intensity peaks, indicating that a single exciting source or a cluster of exciting sources smaller than the beam provides the energy for the far-IR emission. The 40–180 μm spectra (Fig. 1) are very poorly fitted by single blackbody or dilute blackbody models. There is also considerable variation in spectral shape from source to source which the 60–100 μm color temperatures in Table 3 do not reflect.

ii) *Source Geometry*

Cloud models for sources similar to the cores studied here with uniform or monotonically decreasing densities result in large changes in apparent source size from 60 μm to 180 μm (e.g., Scoville and Kwan 1976). The absence of such changes implies either a grain population with large variations in emissivity over this wavelength range or a highly non-uniform geometry. Two possible geometries are dust shells that are optically thick at the wavelength of the heating radiation and

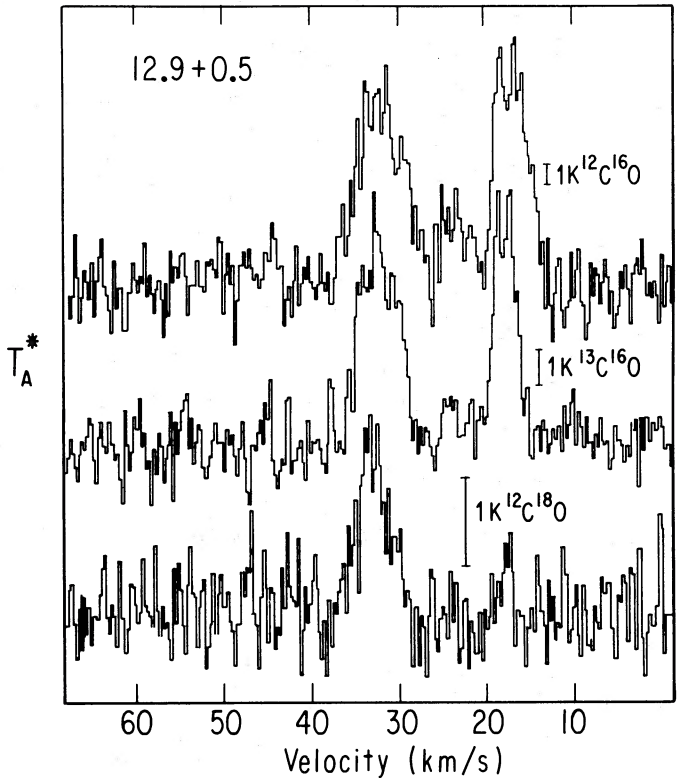

FIG. 6a

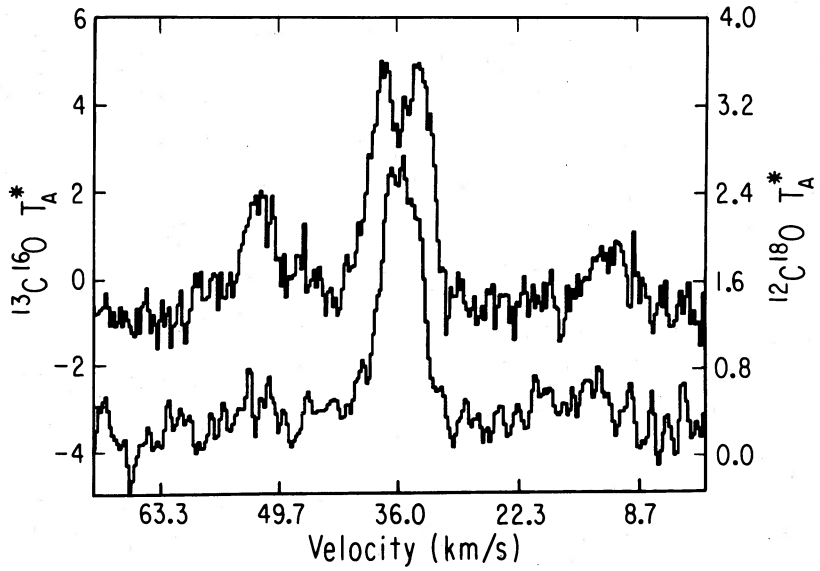

FIG. 6b

FIG. 6.—(*a*) CO spectra toward far-IR 12.9+0.5. The small bars give the vertical scale for the different isotopic species. (*b*) $^{13}C^{16}O$ (*top*) and $^{12}C^{18}O$ (*bottom*) spectra toward a point 7″ west and 54″ north of the far-IR position for W33A.

sources consisting of clumps that are optically thick at the wavelength of the heating radiation.

Whatever the geometry, the constant source size from 60 μm to 400 μm and the absence of any significant shifts in source position with wavelength over this range indicate that the heating sources coincide with peaks in the density distribution in all of the sources we observed. In all cases, the 180 μm flux 63″ from the source center is 0–25% of the peak value. Given the measured source sizes (Table 1) and the 51″ beam size, this measurement implies volume densities at least an order of magnitude higher in the cores of the sources than in the surrounding cloud.

iii) *Diffuse Far-IR Emission from* H II *Regions*

In our study of the far-IR source 14.43−0.69 (§ III), which lies next to the radio continuum source 14.45−0.66, we resolv-

ed one puzzle from the JSF survey: the nondetection of far-IR emission from 33 weak extended radio continuum sources from the catalog of Altenhoff *et al.* (1978). The 21 far-IR sources in the survey sample that had 10.7 GHz counterparts with measured sizes had a mean ratio of radio continuum to far-IR diameter of 1.8 ± 1.2. JSF suggested that the radio excesses and larger radio sizes were due to the low far-IR surface brightness of the radio continuum sources. The radio continuum source 14.45−0.66 was not detected at 70 μm by JSF. It has a 10.7 GHz size larger than the far-IR size of 14.43−0.69 (3′ vs. 1′). Its 10.7 GHz flux is 1200 mJy. In order to test the suggestion of JSF, we made a partial map of the radio source at 185 μm with an 87″ beam. We detected emission at all the positions we examined (principally a north-south strip 1′ west of the radio continuum peak (see the radio and 120 μm maps in Fig. 3). Therefore, the source extent may be so large that we did not chop completely off of the source, even with a 9′ east-west chopper throw. The uniform brightness along our scan out to $\pm 5'$ indicates either that the far-IR source associated with radio continuum source is considerably larger than the radio source or that the far-IR emission comes primarily from a shell around this source. We have also measured the 100 μm flux from a position 1′ west and 1′ north of the radio peak. The 100 μm/185 μm flux ratio at this point implies a blackbody color temperature of 48 K for the diffuse emission. If we add up the 185 μm flux from the eight points we observed and assume a 48 K dust temperature, we derive a luminosity of 5.5×10^4 $L_\odot$. The total source luminosity will be ~ 2 times larger if the far-IR emission extends out to the 10% contour of the radio map. From the 10.7 GHz flux we derive a value for the number of Lyman continuum photons absorbed by the gas of 6×10^{47}, which implies a luminosity of 4×10^4 $L_\odot$ if a single ZAMS O9 star provides these photons (Panagia 1973) and 8×10^4 $L_\odot$ if a cluster of three identical ZAMS stars supplies the photons.

The measured 185 μm surface brightness and 100 μm/185 μm temperature of the diffuse emission implies that the emission would have been present at ~ 4 times the rms noise in the JSF survey. The observed extent of the emission would have brought the source below the 3 σ limit of the JSF observations, since the chopper throw used in the earlier observations was only 5′ and the source selection criteria favored weak point sources over weak extended sources (Stier *et al.* 1982). The 185 μm observations confirm that thermal radio sources like 14.45 − 0.66 emit energy in the far-IR consistent with the luminosities inferred from the radio continuum measurements and that the far-IR sources have sizes comparable to or larger than the radio sources.

b) *Near-IR Properties*

Table 8 gives the parameters of detected near-IR sources in the eight far-IR fields and 10 μm upper limits and sizes of the areas scanned for undetected sources (from Jaffe 1980, and other references). Only two of the eight far-IR sources (W33A and 14.4−0.7) have 10 μm flux densities greater than or equal to 9 Jy. The remaining six have no 10 μm counterparts in 2′ boxes centered on the positions listed in Table 7. In the complete 10 μm survey of the 42 far-IR sources in the JSF sample, at the same time limit, Jaffe (1980) detected 10 μm sources toward only two additional far-IR sources: W33 and M17. Beichman (1979) detected a counterpart to 12.4+0.5, and Downes *et al.* (1984) detected a counterpart to W33B at 20 μm. The 10 μm fluxes for both of these sources lie below the limit of the Jaffe (1980) survey. W33A was also detected in the near-IR prior to that survey (Dyck and Simon 1977).

The results of Downes *et al.* (1984) provide a plausible prediction of the near-IR properties of the far-IR selected sources. They searched to low levels at 20 μm (1–2 Jy) for continuum emission from H_2O maser centers in luminous star formation regions and detected sources in 17 of 21 regions. The detected sources have cool 20–30 μm colors and, where detected at shorter wavelengths, have hot 3.5–12.5 μm colors and deep silicate features. Since $\geq 50\%$ of the sources in the JSF survey and seven of eight of the sources in the present subsample have associated H_2O maser emission, we would expect many near-IR counterparts to be of this type (i.e., similar spectral shape to W33A, but fainter at $\lambda \leq 12.5$ μm). The 10 μm fluxes from these sources will be 10–100 times lower than the survey limit of Jaffe (1980).

c) *Radio Continuum Emission*

The 42 far-IR sources in the JSF survey have luminosities equal to those of single ZAMS late O to early B stars. Such stars would emit sufficient numbers of Lyman continuum photons to produce H II regions with observable radio continuum emission around all of the far-IR sources. A substantial fraction ($\sim 25\%$) of the JSF sources have little or no detectable

TABLE 8

NEAR-INFRARED RESULTS AND UPPER LIMITS

Source (1)	Source Position or Location of Search Box Center R.A. (1950) (2)	Decl. (1950) (3)	Position Error of Detected Sources (arcsec) (4)	Box Size of Undetected Sources (arcmin square) (5)	Broad Band 10 μm Flux Density (Jy) (6)	20 μm Flux Density (Jy) (7)	References (8)
12.4+0.5.....	18^{h}07^{m}55^s.8	−17°56′32″	3	...	4	50	1, 2
12.9+0.5.....	18 08 58.4	−17 32 26	...	2.0	<8[a]	...	3
12.8+0.3.....	18 09 17.4	−17 42 36	...	2.5	<9	...	3
12.7−0.2.....	18 10 59.2	−18 02 40	2	...	...	5	4
12.9−0.3.....	18 11 43.7	−17 53 02	5	...	15	114	5, 6
12.4−1.1.....	18 13 56.0	−18 42 40	...	2.0	<4	...	3
14.3−0.6.....	18 15 59.2	−16 48 48	...	2.0	<9	...	3
14.4−0.7.....	18 16 24.2	−16 45 17	5	...	9	33	3

[a] Upper limits for undetected sources are 1.5 times the peak to peak noise in the maps.

REFERENCES.—(1) Beichman 1979. (2) Wright 1983. (3) Jaffe 1980. (4) Downes *et al.* 1984. (5) Capps, Gillett, and Knacke 1978. (6) Dyck and Simon 1977.

10.7 GHz continuum emission at levels a factor of 3–20 below those predicted for single ZAMS stars. Another 10%–15% of the sources have no compact radio counterparts but exhibit weak 10.7 GHz emission over an area much more extended than the far-IR emission. JSF proposed that the first class of sources were probably clusters of ZAMS stars which would have the same luminosity as the single star but far lower Lyman continuum fluxes. The high densities in the cloud cores and the coincidence of the hottest dust and the H_2O maser emission sites with density peaks, however, suggest the presence of younger, luminous *pre*–main-sequence objects instead of or in addition to the ZAMS stars. JSF also argued that the extended radio sources were line-of-sight coincidences of compact far-IR sources with older H II regions.

We have examined five of the eight sources in the current far-IR subsample and three additional sources in the 5 GHz continuum with the VLA. Wynn-Williams, Beichman, and Downes (1981) also studied W33A and W33B at 5 GHz with the VLA. Toward each of two far-IR sources, 12.4+0.5 and 14.3−0.6 (Table 6), we detected two 5 GHz sources. With the exception of 12.4+0.5A, which we did not resolve, the sources are extended with respect to the beam and optically thin. In both cases, they were spatially well separated (~5 source diameters). The two sources in 12.4+0.5 can account for 45% ± 18% of the observed single dish flux at 10 GHz with a 70″ beam if the sources are both optically thin or 65% ± 35% if 12.4 + 0.5A is optically thick. We have only an upper limit to the single-dish flux toward 14.3−0.6. We did not detect continuum emission from any of the other sources to the levels given in Table 5.

The suggestion of JSF that clusters of B stars could account for the far-IR luminosity and radio continuum flux sources like 12.4+0.5 and 14.3−0.6 relies on the steep dependence of Lyman continuum photon emission on spectral type in early B stars; while a single ZAMS B0 could account for the luminosity of 12.4+0.5, such a star would emit ~20 times too much Lyman continuum. One B0.5 star and two B1 stars would have the same luminosity and emit an order of magnitude fewer Lyman continuum photons. If we can establish that the observations of 12.4+0.5 (Fig. 5) and 14.3−0.6 really show multiple sources powered by different stars, then we can demonstrate that the JSF hypothesis is reasonable although not necessarily the only correct explanation for the low number of Lyman continuum photons emitted in these regions.

Could a single B0 star ionize both 12.4+0.5A and B and provide the luminosity for the far-IR source? If a B0 star were halfway between 12.4+0.5A and B, these two radio continuum sources would intercept a solid angle $\sim\pi/4$ and absorb $\sim 1/16$ of the Lyman continuum photons from the star. The observed fluxes from the sources are consistent with this model. The single-dish radio observations and the source size and density derived from the submillimeter observations, however, make the postulated single B0 star implausible. The 10.7 GHz observations give a flux of 18 ± 6 mJy, implying $N_L \sim 1 \times 10^{46}$ Lyman continuum photons are absorbed per second in the inner 70″ of the source. The mean electron density n_e for a diffuse H II region filling this volume V is then

$$n_e = \left(\frac{N_L}{\alpha V}\right)^{1/2} \text{cm}^{-3}, \quad (2)$$

where α is the recombination coefficient. This average electron density is ~60 for 12.4+0.5. At the same time, the submillimeter data give an average H_2 density over the inner 26″ of the source of 8×10^4 cm^{-3}. In order for this dense neutral material to intercept less than an additional 1/16 of the ionizing radiation, and therefore not to form radio bright rims that would be observable with the VLA, it would have to cover less than 1/16 of the solid angle. There are two problems with this possibility. First, if the dense material intercepted only 1/16 of the UV, it would also intercept only 1/16 of the stellar luminosity. Second, the density in this material would have to be $> 5 \times 10^6$, thus making it impossible for the $n_e \sim 60$ cm^{-3} H II region to confine it. Therefore, a single source of ionization cannot supply the UV photons to both 12.4+0.5A and B. Placing the star closer to one of the compact radio sources makes the problem worse since the star will then have to emit more Lyman continuum photons. Similar arguments apply to the two radio sources in 14.3−0.6. The presence of the multiple radio sources in these regions therefore serves as direct evidence for excitation by stellar clusters rather than single stars.

If the compact H II regions we have detected are spherically symmetric and completely surrounded by neutral material, their ages are $\sim 2 \times 10^3$ yr. This age is short in comparison to the lifetime of the H_2O masers in the same regions (Jaffe, Guesten, and Downes 1981) and to the time it takes early B stars to reach the ZAMS (Iben 1965). Surprisingly short compact H II region lifetimes are a problem in many molecular cloud cores. One picture consistent with the observations is that a cluster of stars with masses up to $\sim 10\ M_\odot$ powers each far-IR source. The most massive stars in each cluster are close enough to the ZAMS to provide the Lyman continuum photons to ionize the observed H II regions. The somewhat less massive stars, which evolve more slowly and therefore are not yet on the ZAMS, provide the remaining observed luminosity and the excitation for the observed H_2O maser sites.

Why did we not detect radio continuum emission from the other sources we observed? One possibility is that the sources were too extended. Our flux sensitivity decreases linearly with source size for sources larger than the beam size (0.″55 by 0.″85). The two sources in 14.3−0.6 are just at the limit of detectability determined by their size and flux. Slightly larger or slightly fainter radio counterparts to other far-IR sources would have been missed. It is interesting to note that the radio source 14.5−0.6, which has a 10.7 GHz flux of 1200 mJy and a size of 3′, has no compact sources detectable at 6 cm with the VLA in the A configuration. Another possibility is that the surface temperatures of the most massive stars in the exciting clusters are not yet high enough to provide sufficient numbers of Lyman continuum photons. A third possibility is that the exciting stars of some of the compact far-IR sources could be pre–main-sequence Brackett line excess stars. These objects, which have been observed as bright near-IR sources in a number of cloud cores, have *excess* Lyman continuum emission for their luminosities, as inferred from Brackett line and far-IR continuum observations (see Thompson 1982). None of these stars has a detectable radio continuum counterpart, albeit at a level somewhat higher than the limits in Table 5.

d) CO *Results*

i) *General Remarks*

JSF found peaks in the brightness temperature distribution of the $^{12}C^{16}O$ $J = 1$–0 line toward only ~60% of the 42 far-IR sources they observed and toward four of the eight sources in the current subsample. The ^{12}CO peaks that did exist were not

very prominent against the extended emission from giant molecular clouds. Often it was either impossible to find the half-power points of the brightness temperature distribution or these points were up to 5′ from the far-IR sources. Typical peak ^{12}CO brightness temperatures were only 15 K. Both this low value of T_B and the large source sizes imply that the surfaces they saw observing the ^{12}CO $J = 1$–0 line are far from the far-IR sources and are not very strongly affected by the presence of the embedded stars. The observed characteristics, therefore, are manifestations of the high optical depth of the ^{12}CO line. Unlike many well-studied star formation regions, the sources we have examined are buried deep enough within the cloud that they are not observable as strong ^{12}CO hotspots.

The present results make it clear that the isotopic variant $^{13}C^{16}O$ $J = 1$–0 transition also has a substantial optical depth toward many of the embedded far-IR sources. $^{12}C^{18}O$ observations of cooler clouds with narrow molecular lines have established that these clouds without luminous embedded objects often have ^{13}CO lines with $\tau > 1$ (cf. Myers, Linke, and Benson 1982). Figures 6*a* and 6*b* illustrate the existence of optically thick ^{13}CO regions in the warmer sources in our subsample as well. Figure 6*a* shows spectra of the 20 km s^{-1} and 34 km s^{-1} components of $^{12}C^{16}O$, $^{13}C^{16}O$, and $^{12}C^{18}O$ toward FIR 12.9+0.5. The two velocity components have almost equal strength in the ^{12}CO and ^{13}CO transitions, but the 34 km s^{-1} component is an order of magnitude stronger in the $C^{18}O$ transition. This change implies a large optical depth (≥ 2) in the 34 km s^{-1} component of the ^{13}CO line. Figure 6*b* shows ^{13}CO and $C^{18}O$ spectra toward a point $\sim 1'$ north of W33A. The dip in the ^{13}CO spectrum at the velocity of peak $C^{18}O$ emission strongly indicates that the ^{13}CO line is self-reversed. This type of spectrum can arise only when both a temperature gradient and a substantial line optical depth are present.

The $C^{18}O$ observations listed in Table 7 also show that the ^{13}CO line may be locally optically thick. The $^{12}C^{18}O$ optical depths range from 0.06 to 0.18, which would imply a range in $^{13}C^{16}O$ optical depths from 0.75 to 2.25, assuming a solar ratio for $^{16}O/^{18}O$ and assuming $^{12}CO/^{13}CO = 40$. These optical depths are probably lower limits, since they assume $T_{ex} = T_{dust}$, where T_{dust} is the 60–100 μm νB_ν color temperature listed in Table 3, and yet T_B for ^{13}CO $J = 1$–0 is much less than T_{dust} (i.e., the ^{13}CO line comes from cooler gas distant from the heating sources). Even higher local optical depths could result if the gas is clumpy or the density peaks sharply toward the source center. Consequently, we have chosen to use $C^{18}O$ as an optically thin probe of the molecular gas.

The $C^{18}O$ observations of the far-IR sources show the following:

1. For the sources we studied, the mass of material within 30″ of the source positions, based on an average of the Taurus and Ophiucus $C^{18}O$ abundances of Frerking, Langer, and Wilson (1982), is 700–9000 $M_\odot$ (Table 7). These masses are consistently 3–4 times more than the masses derived from the submillimeter observations (Table 4). This scaling difference is not significant, given the factor of 2 range in systematic errors involved in calibrating each type of mass estimate.

2. The $C^{18}O$ sizes of the sources we mapped (12.4+0.5, 12.9 + 0.5, W33A, and W33B) are larger than the 180 μm or 400 μm sizes. We discuss the reason for this below.

3. The densities derived from the $C^{18}O$ observations range from 7×10^4 to 2.1×10^5. The high values imply $T_{dust} \sim T_{gas}$ in the cores of these sources (Goldsmith and Langer 1978).

ii) *Comparison of* $C^{18}O$ *and Submillimeter Source Sizes*

The main inconsistency between the measurements of the $C^{18}O$ $J = 1$–0 line and the 400 μm dust continuum that cannot be explained as a scaling or calibration error is the difference in the source sizes. For an isothermal source, $C^{18}O$ integrated line strength and 400 μm flux should both be proportional to column density. In the sources where we have mapped both types of radiation (W33A and 12.4+0.5), however, the source sizes differ considerably (26″ at 400 μm vs. 110″ in $C^{18}O$ for 12.4+0.5). The most likely reason for the size difference is the decrease in gas and dust temperature with distance from the center of the source and the different dependence of column density estimates on temperature. If the $J = 1$–0 line of $C^{18}O$ is optically thin, the integrated line strength $\int T_B\, dv$ is given by:

$$\int T_B\, dv = C\, \frac{h\nu_{10}}{kT_{ex}}\, (1 - e^{-h\nu_{10}/kT_{ex}})(T_{ex} - T_{bg})\, \frac{N_{CO}}{N_{H_2}}\, N_{H_2}\,, \quad (3)$$

where $C = (3/16\pi)(c^2/\nu_{10}^2)A_{10}$, ν_{10} is the line frequency, N_{H_2} is the column density of molecular hydrogen, T_{ex} is the line excitation temperature, and T_{bg} is the temperature of the cosmic background. Since $T_{ex} \gg T_{bg}$ and $h\nu_{10} \ll kT_{ex}$ in the present case, we have

$$\int T_B\, dv = C\left(\frac{h\nu_{10}}{k}\right)^2 \frac{N_{H_2}}{T_{ex}}\, \frac{N_{CO}}{N_{H_2}}\,. \quad (4)$$

We have assumed throughout that the CO is thermally populated up to some reasonable level ($J \geq 7$). Over the range of likely dust temperatures in the cores of the far-IR sources (20–60 K), $h\nu$ for sub-mm emission is of the same order as kT. We can approximate blackbody emission by

$$B_\nu(400\ \mu\text{m}) \approx 5.2 \times 10^{-15} T^{1.8}\,. \quad (5)$$

This expression is accurate to better than 10% from 20 K to 60 K. For optically thin submillimeter emission, the flux density $S_\nu(400\ \mu\text{m})$ is related to the solid angle Ω, which is given by the equation

$$\Omega = \frac{\Omega_{source}\,\Omega_{beam}}{\Omega_{source} + \Omega_{beam}} \quad (6)$$

and the ratio of hydrogen column density to 400 μm optical depth α (Hildebrand 1983) by

$$S_\nu(400\ \mu\text{m}) = \alpha\Omega N_{H_2} B_\nu(400\ \mu\text{m})\ \text{W m}^{-2}\ \text{Hz}^{-1}\,. \quad (7)$$

If the excitation temperature and the dust temperature (which are most likely equal) are constant across a source, the source size will be the same whether one observes sub-mm continuum flux from dust or $C^{18}O$ integrated line strength. One would expect, however, that the temperature decreases away from the center of the source. For sources where dust grains dominate the energy transport but the outer part of the cloud is optically thin to reemitted radiation, the temperature will depend only on the distance to the source center, r,

$$T_d \propto r^{-[2/(4+\beta)]}\,, \quad (8)$$

where β is the power of the dust emissivity dependence on wavelength ($\beta = 0$ for a blackbody). Although a Gaussian source model is not realistic for large changes in temperature, we can demonstrate the effect on source size measurements of relatively small changes in source temperature by modeling both the variation of temperature and density with radius as Gaussian distributions. If the density and temperature dis-

tributions have a full width to half power of Θ_n and Θ_T, respectively, the ratio of the CO and sub-mm apparent source sizes is given by:

$$\frac{\Theta_{CO}}{\Theta_{SMM}} = \left(\frac{\Theta_T^2 + \Theta_n^2}{\Theta_T^2 - \Theta_n^2}\right)^{1/2} . \quad (9)$$

If $\Theta_T = 1.3\Theta_n$, then the temperature at the half-power point of the density distribution is still two-thirds of the peak temperature. The ratio of the measured sizes is $\Theta_{CO}/\Theta_{SMM} = 2.3$. More generally, equations (4) and (5) show that any time the density dropoff is not significantly more rapid than the dropoff in temperature, the ratio of sizes measured by observing $C^{18}O$ integrated line strength and by measuring sub-mm flux and assuming a constant temperature will be considerably larger than 1.

A second possible explanation for the difference in the measured sizes is that there is an extended cooler cloud surrounding the warm compact condensation around the source. In addition to the greater prominence of the cool cloud in $C^{18}O$, the small chopper throw used in the sub-mm observations would make these observations less sensitive to extended emission. In order to test this possibility, we took $C^{18}O$ spectra toward the positions of the reference beams for the sub-mm observations, 5′ east and west of FIR 12.4+0.5. The $C^{18}O$ integrated line strength is $<6\%$ (3 σ) of the peak value. It is therefore unlikely that extended molecular emission distorts the $C^{18}O$ size measurement. This observation also adds to the evidence that the condensations around the embedded stars powered by the far-IR emission are dense cores and not slight density enhancements in a large ambient cloud.

V. SUMMARY AND CONCLUSIONS

The observations of our sample of compact far-IR sources show:

1. Most sources show no significant increase in source size with wavelength from 60 μm to 180 μm.

2. The far-IR spectra are broader than single-temperature blackbodies and vary greatly in shape in spite of the similar 60–100 μm color temperatures of the sources.

3. The large, low surface brightness H II region 14.5−0.7 has associated low surface brightness far-IR emission over a region larger than the radio source. The bolometric flux of this diffuse far-IR emission, scaled to the source distance, equals the luminosity inferred from the radio continuum.

4. The masses derived from the 400 μm emission observed from five of the sources range from 300 to 2400 $M_\odot$.

5. Only two of the eight sources have near-IR counterparts with 10 μm flux densities ≥ 9 Jy. Two additional sources have fluxes below this limit.

6. Two of the five sources observed at 5 GHz with the VLA have associated multiple weak, compact H II regions. The remaining sources were not detected.

7. Both ^{12}CO and ^{13}CO $J = 1$–0 transitions toward the far-IR sources are optically thick.

8. $C^{18}O$ $J = 1$–0 observations imply masses 3–4 times larger than the submillimeter mass estimates. The size scale of $C^{18}O$ regions is considerably larger than the sizes measured at 180 μm or 400 μm.

The near-IR, far-IR, and submillimeter continuum results show that the heating sources coincide with strong density peaks in the objects in our sample. The stars responsible for the luminosity lie deep within the cores. As a result, the sources are much weaker near-IR emitters than many well studied star formation regions. The similar source sizes at 60–400 μm require either a geometry in which the dust temperature drops only slowly with radius, one where optically thick clumps allow a range of temperatures at each radius, or a relatively empty cavity surrounded by a shell with a steep temperature gradient.

The radio continuum results indicate that clusters of ZAMS and pre–main-sequence B stars can account for both the radio emission and the far-IR luminosity. In some cases where no radio continuum emission is observed, all of the exciting stars could be pre–main-sequence stars—either stars which are not emitting ionizing radiation *or* stars with dense ionized envelopes that emit large amounts of radiation in hydrogen recombination lines like Brγ. In the two sources where we detected 5 GHz emission, the observations strongly suggest the presence of more than one ionizing star. As in the JSF results, W33A remains outstanding as a source with too little radio continuum emission for its luminosity. It remains one of the best examples of a high-luminosity far-IR source powered by a pre–main-sequence star or star cluster.

Like the sub-mm results, the $C^{18}O$ observations imply densities in the cores of the sources high enough to make $T_{dust} \sim T_{gas}$ (0.7–2.1 $\times$ 10^5 cm^{-3}; see Table 7). A gradient in temperature can explain the differences between the sizes measured in the sub-mm and in $C^{18}O$. It is hard to reconcile the 60–400 μm size information with the $C^{18}O$ and 400 μm size relation, however, unless there is material at $T < 25$ K outside the warm shell seen in the far-IR.

We thank E. E. Becklin, M. Dragovan, W. Glaccum, S. H. Moseley, R. Pernic, J. Smith, and M. W. Werner for valuable assistance. This work was supported in part by NASA grants NSG 2057 and NGR 14-001-227 and NSF grant AST 81-17134 to the University of Chicago.

APPENDIX

DERIVATION OF FAR-IR FLUX DENSITY

For each filter/aperture combination used on a given night, we made observations both of the program object and of a calibration object (M82 in 1981 and Callisto or Mars in 1982). A spectrum $I_{CAL}(\nu)$ had been calculated previously for M82 using the procedure outlined here to compare the calibrator repeatedly to planets with known brightness temperatures (D. A. Harper 1983, private communication). For Mars, we used the brightness temperature model of Wright and Odenwald (1981) to calculate the fluxes. For Callisto, we assumed a brightness temperature of 140 K (Loewenstein *et al.* 1982). The measured signal for the calibration object through the ith filter/aperture combination P_i(CAL) is

$$P_i(\mathrm{CAL}) = R \int_0^\infty I_{CAL}(\nu) F_i(\nu) A(\nu, W) d\nu , \quad (A1)$$

where R is an instrumental gain factor, $F_i(\nu)$ is the filter/aperture response function, including diffraction effects, and $A(\nu, w)$ is the atmosphere transmission at a given line-of-sight water vapor level W. The expression for the signal measured from the program object is identical to equation (A1) except that we break $I_{\rm OBJ}(\nu)$ into two components, an intensity scale factor C_i and a spectral shape $J_{\rm OBJ}(\nu)$, such that $\int_0^\infty J_{\rm OBJ}(\nu)d\nu \equiv 1$. Thus,

$$I_{\rm OBJ}(\nu) = C_i J_{\rm OBJ}(\nu) . \tag{A2}$$

In the nth iteration, we then find

$$C_{i(n)} = \frac{P_i(\rm OBJ)}{P_i(\rm CAL)} \frac{\int_0^\infty I_{\rm CAL}(\nu)F_i(\nu)A(\nu, W)d\nu}{\int_0^\infty J_{{\rm OBJ}(n-1)}(\nu)F_i(\nu)A(\nu, W)d\nu} , \tag{A3}$$

where $J_{{\rm OBJ}(n-1)}(\nu)$ is the spectral shape derived from the previous iteration. In the initial iteration we choose

$$J_{\rm OBJ}(\nu) = \frac{B_\nu(T)}{\int_0^\infty B_\nu(T)d\nu} \tag{A4}$$

with $T = 50$ K. In subsequent iterations we construct a spectrum from a spline fit to the results of the previous iteration. Usually three or four iterations are sufficient for all of the C_i's to converge to a constant value; that is, the spectral shape does not change with further iteration. We then define the frequency equivalent effective wavelength of each filter as

$$\lambda_{i(\rm eff)}^{-1} = C^{-1} \frac{\int_0^\infty \nu[I_{\rm OBJ}(\nu)F_i(\nu)A(\nu, W)]d\nu}{\int_0^\infty I_{\rm OBJ}(\nu)F_i(\nu)A(\nu, W)d\nu} \tag{A5}$$

and the observed flux density as $I_{\rm OBJ}(\nu_{\rm eff})$.

REFERENCES

Altenhoff, W. J., Downes, D., Pauls, T., and Schraml, J. 1978, *Astr. Ap. Suppl.*, **35**, 23.
Beichman, C. A. 1979, Ph.D. thesis, University of Hawaii.
Capps, R. W., Gillett, F. C., and Knacke, R. F. 1978, *Ap. J.*, **226**, 863.
Downes, D., Genzel, R., Becklin, E. E., and Wynn-Williams, C. G. 1984, in preparation.
Dyck, H. M., and Simon, T. 1977, *Ap. J.*, **211**, 421.
Evans, N. J., II, Blair, G. N., Nadeau, D., and Vanden Bout, P. 1982, *Ap. J.*, **253**, 115.
Frerking, M. A., Langer, W. D., and Wilson, R. W. 1982, *Ap. J.*, **262**, 590.
Goldsmith, P. F., and Langer, W. D. 1978, *Ap. J.*, **222**, 881.
Goldsmith, P. F., and Mao, X. J. 1983, *Ap. J.*, **265**, 791.
Harper, D. A. 1984, Glaccum, W., Loewenstein, R. F., and Pernic, R. 1984, in preparation.
Harper, D. A., Hildebrand, R. H., Stiening, R., and Winston, R. 1976, *Appl. Optics*, **15**, 53.
Hildebrand, R. H. 1983, *Quart. J.R.A.S.*, **24**, 267.
Hildebrand, R. H., Loewenstein, R. F., Harper, D. A., Keene, J. B., Orton, G. S., and Whitcomb, S. E. 1984, in preparation.
Ho, P. T. P., Martin, R. N., and Barrett, A. H. 1981, *Ap. J.*, **246**, 761.
Iben, I. 1965, *Ap. J.*, **141**, 993.
Jaffe, D. T. 1980, Ph.D. thesis, Harvard University.
Jaffe, D. T., Guesten, R., and Downes, D. 1981, *Ap. J.*, **250**, 621.
Jaffe, D. T., Stier, M. T., and Fazio, G. G. 1982, *Ap. J.*, **252**, 601 (JSF).
Kuhn, P. M., Magaziner, E., and Stearns, L. P. 1976, *Geophys. Res. Letters*, **3**, 529.
Lada, C. J., Blitz, L., Reid, M. J., and Moran, J. M. 1981, *Ap. J.*, **243**, 769.
Loewenstein, R. F., Harper, D. A., Hildebrand, R. H., Keene, J., and Whitcomb, S. 1982, *Bull. AAS*, **14**, 612.
Myers, P. C., Linke, R. A., and Benson, P. J. 1983, *Ap. J.*, **264**, 517.
Panagia, N. 1973, *A.J.*, **78**, 929.
Scoville, N. Z., and Kwan, J. 1976, *Ap. J.*, **206**, 718.
Stier, M. T. 1979, Ph.D. thesis, Harvard University.
Stier, M. T., Jaffe, D. T., Fazio, G. G., Roberge, W. G., Thum, C., and Wilson, T. L. 1982, *Ap. J. Suppl.*, **48**, 127.
Thompson, R. I. 1982, *Ap. J.*, **257**, 171.
Thronson, H. A., and Harper, D. A. 1979, *Ap. J.*, **230**, 133.
Ulich, B. L., and Haas, R. W. 1976, *Ap. J. Suppl.*, **30**, 247.
Whitcomb, S. E., Hildebrand, R. H., and Keene, J. 1980, *Pub. A.S.P.*, **92**, 863.
Whitcomb, S. E., and Keene, J. 1980, *Appl. Optics*, **19**, 197.
Wright, E. L. 1983, preprint.
Wright, E. L., DeCampli, W., Fazio, G. G., Kleinmann, D. E., and Lada, C. J. 1979, *Ap. J.*, **228**, 439.
Wright, E. L., and Odenwald, S. 1980, *Bull. AAS*, **12**, 456.
Wynn-Williams, C. G., Beichman, C. A., and Downes, D. 1979, *A.J.*, **86**, 565.

D. A. HARPER and R. F. LOEWENSTEIN: Yerkes Observatory, Williams Bay, WI 53191

R. H. HILDEBRAND: Enrico Fermi Institute, 5640 Ellis Avenue, Chicago, IL 60637

D. T. JAFFE: Space Sciences Laboratory, University of California, Berkeley, CA 94720

JOCELYN KEENE: Downs Laboratory of Physics, California Institute of Technology 320-47, Pasadena, CA 91125

J. M. MORAN: Harvard-Smithsonian Center for Astrophysics, 60 Garden Street, Cambridge, MA 02138